AIAA 97-2378

Laser-Induced Fluorescence Measurements of OMS and LR91 Amine Rocket Exhausts

C. W. Brasier, J. A. Drakes, K. M. Anspach, R. G. Porter, M. A. Simmons, and D. W. Pruitt
Sverdrup Technology, Inc., AEDC Group
Arnold Engineering Development Center
Arnold Air Force Base, Tennessee 37389

19980608 107

28th Plasmadynamics and Lasers
Meeting & Exhibit
June 23-25, 1997 / Atlanta, GA

DISTRIBUTION STATEMENT A

Approved for public release;
Distribution Unlimited

DTIC QUALITY INSPECTED 3

LASER-INDUCED FLUORESCENCE MEASUREMENTS OF OMS AND LR91 AMINE ROCKET EXHAUSTS*

C. W. Brasier, J. A. Drakes,** K. M. Anspach,† R. G. Porter, M. A. Simmons,** and D. W. Pruitt†
Sverdrup Technology, Inc., AEDC Group
Arnold Engineering Development Center
Arnold Air Force Base, TN 37389-9013

Abstract

Nonintrusive diagnostics are often sought to provide information on combustion exhaust flows due to the harsh environment of the flow. Laser-induced fluorescence (LIF) is one technique in which a chosen flow molecule or marker is probed to yield gross flow properties such as static temperature and flow velocities. The work presented herein describes application of LIF to the combustion exhausts of two full-scale liquid-propellant rocket engines, i.e., the Space Shuttle Orbital Maneuvering System (OMS) and the Titan second-stage LR91 rocket engines, as they undergo routine testing in simulated altitude test cells. The method is based upon the use of cw ring-dye lasers which scan in frequency over either the Na D_1 or D_2 line at 5896 and 5890 Å. Na is used as a basis for this approach since it occurs as a trace element in both hydrogen and amine rocket fuels. The generic apparatus is described, including a discussion of the collection and interpretation of the LIF signal to yield radial and temporal profiles of radial flow velocity and static temperature. CFD modeling of the plumes was used to provide baseline estimates of the exhaust flow properties. It was found that the CFD model does a fairly good job of predicting the gross behavior of the flow, although some items of fine spatial structure are not reproduced well. The OMS and LR91 rocket engine nozzles are drastically different in construction and cooling method. It was found that excellent LIF results were obtained with the radiation-cooled nozzle (OMS), while the fuel-film cooling (FFC) used for the LR91 nozzle generated an optically thick and particle-laden region which severely impeded the determination of static temperature from the Na LIF measure-

ments. Ancillary optical scattering measurements were made on the LR91 which indicated the existence of an annulus of particles in the flow periphery. The absolute attenuation of the laser beam was used to deduce the identity of the particles as unvaporized fuel droplets.

Introduction

Nonintrusive optical diagnostics of rocket engine exhausts can provide crucial information on injector performance, nozzle performance, and nozzle integrity. In particular, laser-induced fluorescence (LIF) can provide point measurements of the exhaust flow parameters which may be used to resolve such issues as the extent of propellant mixing and effectiveness of nozzle film cooling. It has been shown that for amine fuels, as well as H_2, sodium is an inherent trace species due to the leaching stage of the production of the fuel.[1-2] Given that sodium has a large optical cross section, and that fluorescence lines occur at the easily accessible wavelengths of 5890 and 5896 Å, it makes an ideal tag for the flow properties. Thus, a Na-based LIF diagnostic technique was developed for full-scale testing at Arnold Engineering Development Center (AEDC) to determine rocket exhaust flow temperature, velocity, and relative fuel distribution.

The potential of LIF measurements has been shown repeatedly in many laboratory and subscale experiments.[3-7] However, measurements have been recently made on two full-scale rocket engine systems while they were undergoing simulated altitude testing. The engines were the Space Shuttle Orbital Maneuvering System (OMS) engine which

---

American Institute of Aeronautics and Astronautics

DTIC QUALITY INSPECTED 3

was tested at NASA's White Sands facility and the Titan IV second-stage LR91 engine which was tested at the AEDC. Both engines used storable propellants, as indicated in Table 1, and were tested at simulated altitude. However, there is considerable difference in engine thrust, area ratio, exit diameter, and nozzle cooling.

Table 1. Characteristic Parameters of OMS and LR91 Rocket Engines

	OMS	LR91
Fuel	MMH	AZ50
Oxidizer	N_2O_4	N_2O_4
Nominal O/F	1.6	1.8
Nominal Thrust, lb	6,000	105,000
Nominal Chamber Pressure, psia	130	850
Nozzle Exit Diameter, cm	110	168
Nozzle Cooling Method	Radiation	Fuel-Film
Area Ratio	55	49
Test Location	NASA White Sands	AEDC
Test Simulated Altitude, km	33	25
Number of Firings	14	3

The essence of the LIF diagnostic method as developed at AEDC for storable propellant rocket engines is the reliance upon the Na inherently present in the amine fuels, i.e., the MMH in the OMS engine and the AZ50 in the case of the LR91, as a result of the fuel manufacturing process which utilizes sodium hypochlorite.[1-2] During the combustion of the fuel, the atomic Na is chemically released, making it an ideal tracer to identify the spatial disposition of the fuel in the flow. Furthermore, the optical cross section of Na is very large, requiring only minute quantities of Na to generate measurable LIF signals.[8] Previous applications of the LIF technique in rocket exhaust plumes demonstrated success with as little as 1 part per billion of Na.[9]

The LIF measurement technique reported here uses a continuous-wave (cw) laser beam that is propagated across the exhaust flow and frequency tuned in a controlled fashion in a range about the frequency of the Na fluorescence line. The cw laser used in these test programs has a line width of 500 kHz. This implies that the cw laser acts as a very fine probe of the spectral structure of the Na fluorescence line which has a nominal width of 1 to 2 GHz, or 10^3 times the laser width, in these applications. As the laser is tuning, portions of the flow will fluoresce to a stronger or lesser extent, depending upon the Doppler-induced frequency shift of the fluorescence line with respect to the laser frequency. Thus, by using a standard video camera operating at a frame rate of 30 frames/sec, it is possible to capture the spatially resolved LIF signal with each video frame corresponding to an average of laser frequencies over the frame integration time interval. For example, if a 30-GHz laser scan requires a 5-sec time interval, then the frequency interval averaged in a single video frame is roughly 0.2 GHz. From the video sequence, the spectral shape of the fluorescence line can be reconstructed for each spatial point in the flow. The shape and spectral shift of the spectral line will be used to determine the radial velocity and temperature of the flow.

A program was conducted at the NASA/ Johnson White Sands Test Facility (WSTF) in New Mexico to measure radiative and flow-field properties at the exhaust of a Shuttle Orbital Maneuvering System (OMS) engine. This program was sponsored by the Strategic Defense Initiative Organization (SDIO) through the Phillips Laboratory at Edwards Air Force Base, California. The objectives were to obtain diagnostic data for engine and nozzle flow-field code validation. The OMS engine was tested in Test Cell 403 at the WSTF, which is a steam-pumped test facility capable of testing engines at simulated altitudes up to 40 km. The OMS engine is a pressure-fed, fixed-thrust, regeneratively cooled system with multiple start and gimbaling capability and uses nitrogen tetroxide (N_2O_4) and monomethylhydrazine (MMH) as propellants. The exhaust nozzle has a 14.8-cm-diam throat and a 109.5-cm-diam exit which provides an expansion ratio of 55:1. The divergent nozzle incorporates a bell contour with an 8.4-deg half-angle and is 146 cm long from throat to exit. The expansion cone is radiation cooled from an area ratio of 6:1 and is fabricated from columbium alloy FS-85. For purposes of this work, only test OFL2-6 will be reviewed out of the entire 14-test sequence. The specific parameters for this test are given in Table 2.

A simulated altitude nozzle certification test for a nozzle skirt extension to the LR91-AJ-11 rocket engine using a recently developed Low-Density

Table 2. Specific Test Conditions for OMS and LR91 Rocket Engines

Test Identifier	OMS OFL2-6	LR91 Test 2	LR91 Test 3	LR91 Test 4
Nozzle Material	Columbium Alloy	Asbestos	Quartz	Quartz
Chamber Pressure, psia	131	847	868	867
Oxidizer Flow, lbm/sec	11.8	198	211	211
Fuel Flow, lbm/sec	7.2	119	117	120
O/F	1.65	1.67	1.80	1.76
Burn Time, sec	168	20	275	300
FFC Level, % of Total Fuel Flow	N/A	16.7	16.7	13.6

(LD) quartz phenolic liner was conducted in the J-4 Development Test Cell at AEDC. The test program was conducted using both nozzle skirt extension liner materials, the original asbestos phenolic and the LD quartz phenolic. Both nozzle liners rely on considerable fuel-film cooling (FFC) for protection. The LR91 is a large, amine-fueled rocket engine used as the second stage of the Titan IV launch vehicle which achieves a thrust level of nominally 105,000 lbf. The basic LR91 engine is constructed with a thrust chamber integrated with a regeneratively cooled nozzle that expands to an area ratio of 12. Inside the chamber there are 7 axial internal baffles which are cooled by flowing N_2O_4 through them which then sprays into the combustion chamber at the bottom of the baffles. At positions where the baffles are joined to the wall and in the center where the baffles join together, the baffles use fuel cooling rather than oxidizer. A nozzle skirt extension is used in conjunction with the basic chamber nozzle combination that continues the flow expansion to an exit diameter of 168 cm and an area ratio of 49.2:1. The axial length of the nozzle and skirt extension from the throat to the exit plane is 183 cm. The nozzle and skirt extension liner is film cooled, with approximately 16 percent of the total fuel flow being dedicated to film cooling, as noted in Table 2. Note that 12 percent is used for cooling the chamber walls, while the remainder is used for cooling of the baffles. For this work, data from all three LR91 tests will be presented.

Apparatus

The basic LIF system is shown schematically in Fig. 1 and the components are described in Table 3. The system consists of an Ar-ion pump laser, a ring dye laser, a fiber-optic cable to transport the beam into the test cell, a fiber-optic cable head unit located within the test cell, and an absorption detector. The output beam of the pump laser was used to drive a Coherent 699-21 continuous-wave, frequency scanning ring dye laser. The ring dye lasers had the capability of tuning over a 30-GHz frequency interval centered at either the D_1 resonance line of the Na atom at 5896 Å (corresponding to the transition between the $^2P_{1/2}$ state and the ground $^2S_{1/2}$ state) or the D_2 resonance line of the Na atom at 5890 Å (corresponding to the transition between the $^2P_{3/2}$ state and the ground $^2S_{1/2}$ state). After exiting the dye laser, the laser beam was split by a 60/40 beamsplitter into two portions. The weaker portion of the beam was split again, with one beam directed into a Na hollow cathode lamp located on the optics table with the laser, and the other beam directed into a Burleigh WA-2000 wavemeter. The wavemeter measured the gross frequency of the beam, and the Na hollow cathode lamp ensured that the laser frequency was finely tuned to the appropriate Na resonance frequency. The fluorescence generated in the lamp was monitored by a photomultiplier tube, and the output was recorded by a PC-based data acquisition system. Also recorded was the laser scan driving voltage. The second portion of the ring dye laser beam was directed into a fiber-optic coupler that transferred
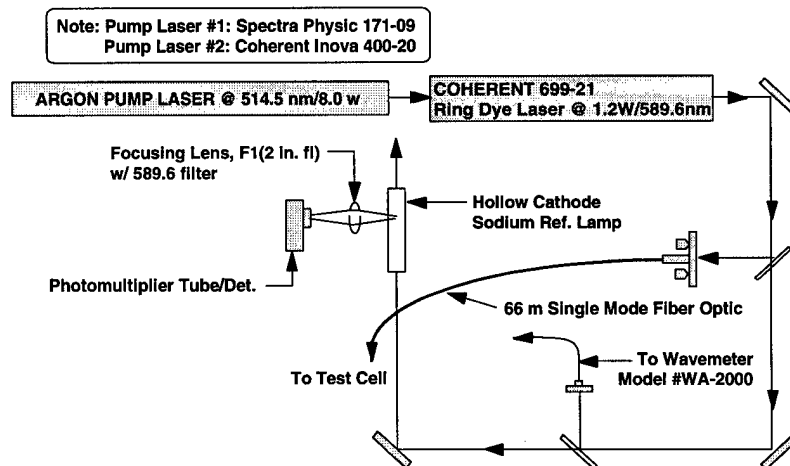

Fig. 1. Na LIF laser system schematic.

Table 3. LIF System Specifications

	OMS	LR91
Pump Laser(s)	Spectra Physics 171-09	Spectra Physics 171-09 Coherent Inova 400-20
Power	7.0 W	8.0W
Center Wavelength	5145 Å	5145 Å
Dye Laser(s)	Coherent 699-21 scanning ring-dye	(2) Coherent 699-21 scanning ring-dye
Dye	Rhodamine 6G	Rhodamine 6G
Linewidth	less than 500 kHz	less than 500 kHz
Power	~1300 mW (out of laser) ~80 mW (out of fiber in test cell)	~1300 mW (out of laser) ~100 mW (out of fiber in test cell)
Frequency Scan Range	30 GHz	30 GHz
Scan Rate	1 scan per 6 seconds	1 scan per 5 seconds
Fiber Optic Cables	(2) 33m, 5 μm-diam, single mode	(2) 66m, 5 μm-diam, single mode
Beam Diameters	5.5 mm on near side of nozzle 9.6 mm on far side of nozzle	4.5 mm on near side of nozzle 8.0 mm on far side of nozzle
Axial Position of Beam	4 in. downstream of nozzle exit	3 in. downstream of nozzle exit 6 in. downstream of nozzle exit
Radial Positions of Beams	Nozzle centerline	From 1 - 10 stations
LIF Visualization Detectors:	1 gain controlled, CCD camera with 5-nm Na line filter	3 gain controlled, CCD cameras with 10-nm Na line filter

the beam into a single-mode optical fiber. The terminus of the fiber was in a fiber-optic head unit also containing a reference power detector. The fiber-optic head unit was placed inside the test cell. On the opposite side of the test cell was a photodiode absorption detector, aligned with the particular laser beam. The voltages from both the reference power and beam absorption photodiodes were also recorded by the PC data acquisition system.

For the OMS test sequence, the cw dye laser tuned across the D_1 absorption line of the sodium atom at 5896 Å. The laser beam was directed across the plume centerline 4 in. downstream of the nozzle exit plane, as shown in Fig. 2. A single gain-controllable, unintensified Dage CCD-72 camera, having an array size of 768 pixels horizontally and 493 pixels vertically with a field-of-view of 54 in. in diameter, was used as the detector. The camera lens was equipped with a 5-nm bandwidth line filter centered on the D_1 line of the sodium atom. The 30-Hz video output of the camera was recorded on VHS tape using a standard recorder.
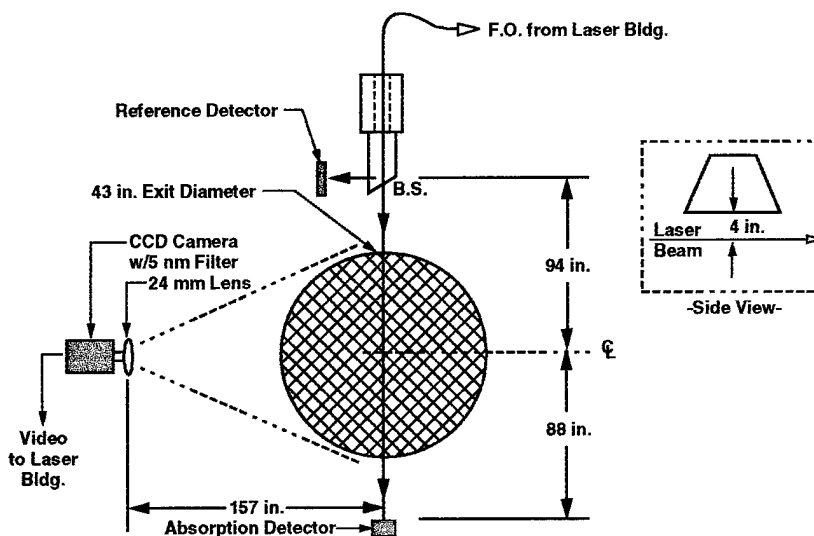
Fig. 2. LIF installation, top view.

Since the LR91 test sequence was potentialy scheduled to have only one firing, it was decided to minimize the risk of data loss by duplicating the measurement. Thus, two complete and independent laser systems which performed redundant tasks were used. These laser systems were installed in an instrumentation building located just outside the test cell. The only difference between the two laser systems was the manufacturer of the pump laser; one system utilized a Spectra Physics 171-09 Argon-Ion pump laser and was referred to as Laser System #1. The second system used a Coherent Inova 400-20 Argon-Ion pump laser, referred to as Laser System #2.

For the LR91, it was desired to traverse the beam across the flow in a plane normal to the plume axis in an attempt to obtain a two-dimensional map of the exhaust flow properties. For Test 3, computer-controlled traversing tables physically translated the fiber-optic head units and the corresponding absorption detectors in a plane normal to the nozzle centerline axis, as indicated in Fig. 3a. The motion began at the nozzle centerline, denoted as Station 1, and proceeded in discrete 10-cm steps outward. The relative orientation of the beams with the cameras was maintained at all times and the beams were traversed to 8 radial stations out to the nozzle boundary (therefore the last radial station was 70 cm from the nozzle centerline). Prior to engine shutdown, the beams returned to Station 1. For Test 4, the fiber-optic head units remained fixed and mirrors were mounted to the traversing carts. The beams were traversed through 10 radial stations in 10-cm increments which extended past the nozzle boundary (to a radial station 90 cm from the nozzle centerline) and the beams did not return to Station 1 prior to shutdown. The traverse position was also recorded on the PC data acquisition system for all tests.

Also differing from the OMS experiments was the detection of the fluorescence with three unintensified Dage CCD-72 array cameras operating at a standard video rate of 30 frames/sec. Each camera was spectrally filtered with a 10-nm bandpass filter centered about the Na fluorescence line. The large size of the LR91 necessitated the use of 10-nm bandpass filters rather than the 5-nm bandpass filters, due to the increased off-axis rejection of the narrower filters. Camera 1 was set with a 24-in.-diam field of view to provide plume boundary viewing, while cameras 2 and 3 had a nominal field of view of 70 in. in diameter to provide full plume diameter viewing, as shown in Fig. 3b. Cameras 1 and 2 utilized computer-controlled zoom lenses to optimize the spatial resolution at each traverse position of the laser beams. Measurements of transmission versus radial position were made on each camera/tilter assembly for each lens setting in order to account for the angular dependence of the overall video response. The video signals from cameras 1 and 2 were sent to the main control room, where they were recorded onto two indepen-
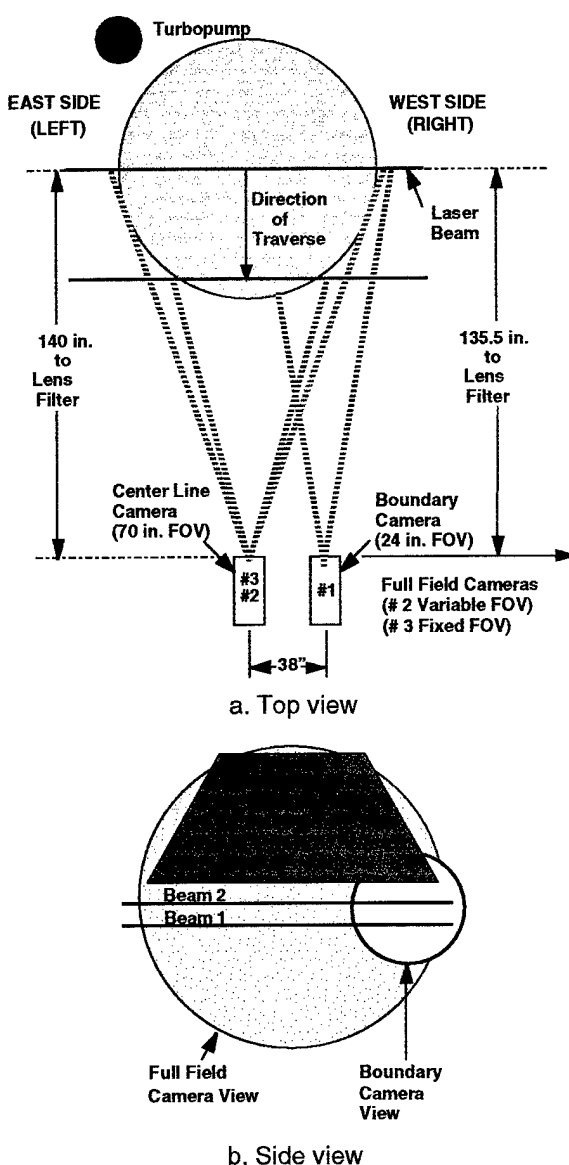

a. Top view

b. Side view

Fig. 3. LIF installation for LR91 testing.

dent Sony D-2 digital recorders. Additionally, the video signals from each camera were fed into the laser area where they were recorded onto three independent Panasonic VHS recorders as a backup. The beam from Laser System #2 was located 3 in. axially downstream of the nozzle exit, while the beam from Laser System #1 was located axially 6 in. downstream of the nozzle exit. In Test 3, the two beams propagated in opposite directions, while in Test 4, they both propagated from the same side.

Data Reduction

Once the imagery was collected on the D2 tape format, it was processed using a real-time digitizer at a resolution of 720 pixels horizontally by 496 pixels vertically. The portion of the image in which the laser signal was apparent was summed in the vertical direction, i.e., a spatial integration over the beam profile, at each horizontal pixel, yielding a LIF signal profile for each image. Note that since the laser scan frequency is correlated with the image, every LIF signal profile is associated with a laser frequency. A correction for the angular response of the system, as well as the variation in the laser power as measured by the reference photodiode, was made to each LIF signal profile.

The background contribution was determined by examining the LIF signal profile at laser frequencies far from resonance. For the OMS, the test cell environment was exceptionally conducive to low background signal, and only small corrections were made to the data. Figure 4 shows a typical raw LIF image from the OMS test during a time when the laser frequency was near the Na fluorescence line center frequency. However, for the LR91, considerable background illumination was present, due in part to test cell lighting for other diagnostic measurements. The 10-nm filters, as opposed to the 5-nm filters used for OMS, gave a higher level of plume visible radiance than the OMS, and numerous objects with highly reflective surfaces near the test article were included. Hence, significant portions of some of the LR91 LIF signal profiles were fatally corrupted by the background.

Once the initial processing of the imagery was complete, the LIF signal profiles were compiled according to laser frequency scans. For the OMS, approximately 165 LIF signal profiles, (5.5 sec times 30 Hz), were acquired during each laser scan. Figure 5 illustrates the set of 165 profiles as a color-map in which the 165-pixel vertical dimension is the laser frequency, the 720-pixel horizontal dimension is the radial location across the plume, and the color indicates the

value of the LIF signal profile. These data were acquired from 79.3 to 84.8 sec of OMS Test OFL2-6. During this laser scan, the laser tuned from −18 GHz (upper edge) to +12 GHz (lower edge), relative to the Na fluorescence line. The physical extent of the horizontal dimension is from −67.3 cm to 69.2 cm, relative to the OMS nozzle centerline. Several features of the fluorescence can be clearly observed from Fig. 5, including the vertical slope of the fluorescence due to the Doppler frequency shift. Note the subtle reverses in the velocity apparent in the image, which will be described in more detail below. Also, the large intensity of the Na fluorescence near the outer edge of the flow is apparent, as well as the narrowing of the frequency line width in the most intense region of fluorescence.

To interpret the LIF signal data, a model of the Na fluorescence profile was created, using standard methods. The model was constructed of two pieces, a first-principles model for the spectral shape of the Na fluorescence line, and a downhill simplex or Nelder-Mead algorithm[10] to optimize the free parameters of the spectral line model, i.e., line width, baseline, amplitude, and frequency shift.
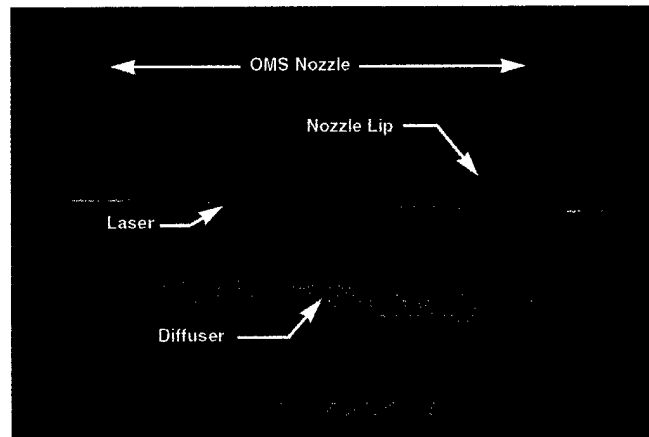

Fig. 4. Raw Image from OMS Firing OFL2-6.

Fig. 5. Fluorescence signal acquired during one laser scan from OMS Test OFL2-6.

Although the capability to vary the relative strength of the transitions between the upper ^2P state and the hyperfine components of the lower ^2S state was originally invoked, the ratio of the hyperfine Na line components was eventually set to the nominal value of 0.375 for the higher energy F_1 line and 0.625 for the lower energy F_2 line.[11] The model used a 1.77-MHz separation between the hyperfine lines. At each of these transitions, a Voigt profile was generated using identical temperatures and broadening parameters. The resulting Na fluorescence line profile was the sum of the two Voigt profiles of the hyperfine components. The entire line profile was then compared to the data. For typical rocket exhausts, the pressures are low, and the line width is expected to be dominated by thermal broadening rather than pressure broadening. In the case of OMS, for example, the nominal broadening parameter based upon computed pressures and temperature (see below) was roughly $\sqrt{\ln 2}(1/62)$. A variation of the broadening parameter was performed, and it was found that the fit results were very insensitive to this variation. Also considered was the saturation broadening of the fluorescence lines, which is relevant when using the line profile to determine the temperature.[12] The saturation parameter is the ratio of the state-specific laser excitation rate to the de-excitation rate due to radiation and/or quenching. The determination of the radial velocity is not impacted by saturation issues; however, saturation can have a significant effect upon the determination of the flow temperature. The impact of the laser saturation will be discussed in more detail below. Items not addressed in the Na fluorescence model were pressure shifting of the fluorescence line and radiative transfer of the emitted fluorescence through the plume.

Prior to the tests, the plume flow field was modeled using standard physics-based Joint-Army-Navy-NASA-Air Force (JANNAF) codes, specifically including the flow properties at the axial locations of the LIF measurements. The thrust chamber was modeled using a methodology similar to the Two-Dimensional Kinetic (TDK) computer program[13] for simulating the spatial flow-field properties and performance of axisymmetric thrust chambers. The solution includes the effects of rate-controlled chemical kinetics and approximates

a viscous boundary-layer flow near the nozzle wall. Nozzle film cooling and nozzle wall ablation effects were not included in this simulation. The chemical equations and kinetic rates included in the simulation are for the primary combustion reactions involving carbon, hydrogen, oxygen, and nitrogen. Reactions involving trace species such as Na would not significantly influence the overall energy and chemistry and were not included. The thrust chamber solution domain commences in the combustion chamber assuming chemical equilibrium conditions, and subsequently performs a finite-rate chemical kinetics solution through the nozzle throat region and the diverging nozzle region. The solution terminates at the nozzle exit plane, providing static temperature, pressure, radial and axial velocity, and chemical composition to be subsequently used as initial starting conditions for the plume expansion model. The simulated nozzle exit plane conditions and the free-stream conditions at the simulated test altitude were provided to the Standard Plume Flowfield computer program.[14] The near-field plume expansion was simulated from the nozzle exit plane to the test cell diffuser location. The objective of the external plume simulation was specifically to obtain the radial velocity and static temperature profiles at axial positions for comparison with the LIF-deduced profiles.

At close proximity to the nozzle exit, the core portion of the flow is most influenced by the nozzle simulation, and measurement comparisons in this region would serve to validate the nozzle solution. However, comparisons with measurements obtained at radial locations in the plume expansion portion of the flow near the outside nozzle lip region would provide an assessment of the initial shear layer development and mixing approximations included in the SPF viscous mixing model. The outer portions of the plume exhaust include the effects of the entrainment of the quiescent test cell air. The phenomenology contributing to the measurements and the modeling of this flow region is the interface of two conditions; in this case a high-velocity plume expansion entraining and merging with a quiescent (ambient velocity approximately zero) and the resulting shear layer development. The shear layer is characterized by a pronounced static temperature peak caused by the

shear stress between the two regions. The radial component of velocity is also influenced dramatically in the shear layer. The shear layer experiences rapid expansion initially, followed by an imposed boundary condition of the quiescent flow region where the radial component of velocity approaches zero. Comparison of the measured LIF profiles in the shear layer region should indicate the accuracy of the initial shear layer profiles and the mixing and entrainment rates of the turbulence approximations.

Results

In the case of the OMS data, the Na fluorescence model was applied to the data, such as that shown in Fig. 5. Figure 6 shows three spectral profiles taken from Fig. 5, at radial positions in the flow of 10.4, 46.5, and 55.9 cm relative to the nozzle centerline. Recall from Table 1 that the nozzle radius is 55 cm; hence, the plume has expanded compared to the nozzle at this axial station. First note that since all three profiles are acquired on the side of the nozzle where the exhaust flow is approaching the laser, the frequency shift is to progressively higher frequencies for positions farther from the nozzle centerline. This is reflected by the radial velocity determined for each spectral profile, as denoted on the figure. Also, note the relative heights of the three spectral profiles where it is seen that the outer region of the flow has a much higher density of Na than does the inner portion. In addition, the structure of the fluorescence is clearly evident for the low-temperature region near the center, where it is possible to discern the two hyperfine components. As the temperature increases toward the outer region of the flow, this structure becomes washed out. Finally, note the excellent agreement of the fit to the data.

During Test OFL2-6, 29 laser scans were obtained. The radial velocity was deduced from the data as described above. Figure 7 displays the radial veloc-

ity observed at three times in the burn, roughly 4, 73, and 120 sec, as a function of radial distance across the plume. It is interesting to note the repeatability of the experimental results at the widely separated times. Also shown on this plot is the result of the calculation. Overall, the agreement of the SPF model with the data is rather good for regions away from the center. Note though, the feature in the data at ± 35 cm which is not evident in the model results. In the region from -20 to 20 cm, there exists a significant discrepancy between the model and the data. Since the difference is symmetric about the nozzle centerline, it suffices to examine the region from 0 to 20 cm. In the portion from 20 to 12 cm, one sees that both the model and the data indicate that the radial component of the flow is proceeding inward toward the nozzle
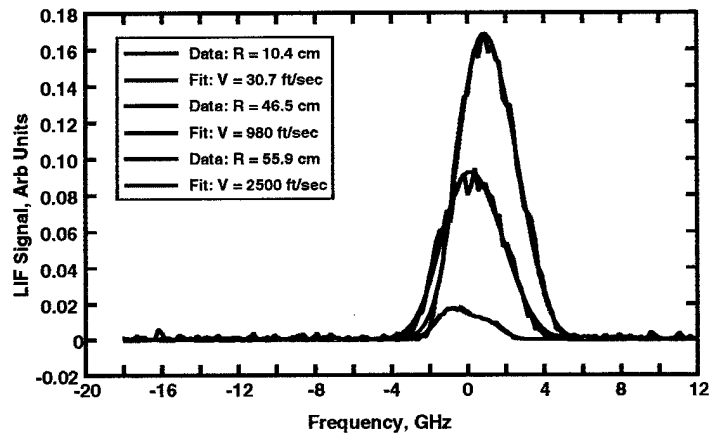

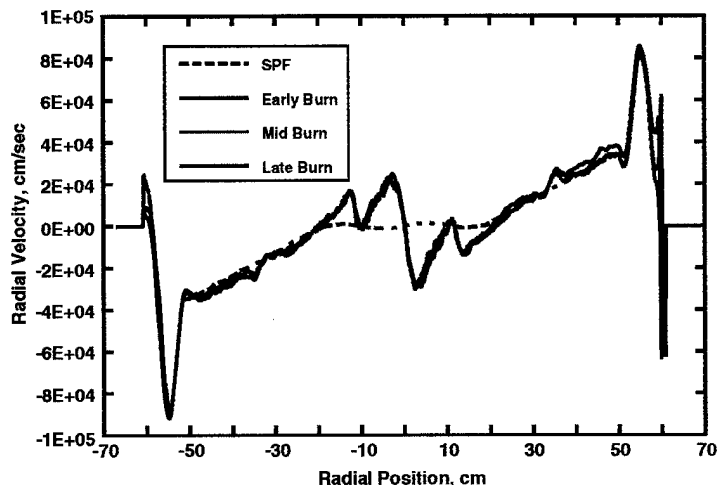Fig. 6. Spectral profiles and fits taken at three radial positions of Fig. 5.

Fig. 7. Measured radial velocities of OMS Test OFL2-6.

axis, rather than expanding outward. However, the data show a much larger magnitude of velocity reversal than the model. Both the model and the data agree that at 12 cm, the flow has a near-zero radial component. However, from 12 to 0 cm, the data indicate that the flow is again toward the nozzle centerline, in qualitative contrast with the model. These discrepancies are much larger than the data uncertainty, which is dominated by the systematic term due to the averaging of the laser frequency during individual video image acquisition. Since the camera averages the fluorescence signal for 33 msec while the laser is continuosly scanning (at a rate of 30 GHz over 5.5 sec for OMS), the systematic radial velocity uncertainty is $\pm 2.5 \times 10^3$ cm/sec.

The results for the exhaust flow static temperature for this test are shown in Fig. 8, as well as the modeling result. The systematic uncertainty due to the frequency averaging yields an uncertainty of $\pm$ 50 K for most of the flow. The prediction is in qualitative agreement with the date in the core flow region. Near the flow axis the prediction is only slightly lower than the data, but the agreement worsens significantly farther from the plume centerline. Since the laser power was moderately high, the temperature determination may be influenced by laser saturation and this possibility is currently being examined. As a function of time, the plume core is seen to be extremely steady, as indicated by the three temperature profiles taken at different times of the burn.

There is a qualitative disagreement of the data with the model near the shear layer interface. The data indicate a temperature maximum roughly 5 cm closer to the nozzle axis than the model prediction. Furthermore, the data show a significant reheating of the outer periphery of the flow. This outer heating is better detected in Fig. 9. In this image, the horizontal dimension is again the radial position across the plume. The vertical dimension is time, starting with the engine ignition at the top of the image, and proceeding downward to

shutdown at the bottom of the image. Each discrete horizontal line in the image corresponds to the temperature profile, as in Fig. 8, for a given laser scan at the specified time. While the core flow is observed to be rather stationary in time, the boundary of the flow shows an increase in the flow temperature as the burn progresses. This is most noticeable in the boundary on the right side of the image. It is suspected that this rate of temperature increase of the exhaust gas may be traceable to the nozzle wall heating temporal profile.

The LR91 test results are quite different from those obtained in the OMS engine. This is due primarily to the difference in the nozzle cooling mechanism, in which the LR91 relied upon heavy amounts of fuel-film cooling. Since Na is a trace species of the fuel, the heavy FFC led to very significant Na densities in the boundary layer of the exhaust flow. In fact, from reviewing the data, it is evident that the plume structure can be categorized into three distinct annular regions. The outermost region was thin, ~ 1 cm, and contained a Na density that led to reasonable fluorescence measurements. Inward of the thin sheath was a ~ 10-cm region of very high Na density, as well as particu-
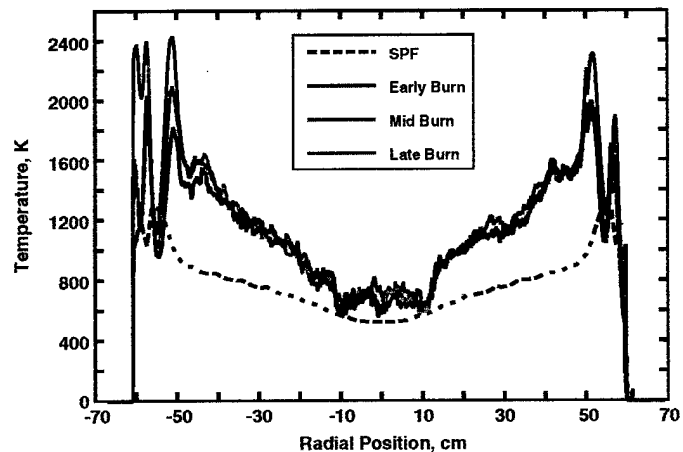

Fig. 8. Measured gas static temperatures of OMS Test OFL2-6.

Fig. 9. Time history of the flow temperature of OMS Test OFL2-6.

lates, which was directly attributable to the nozzle FFC. The remaining core of the exhaust flow could again be characterized as having suitable Na densities for fluorescence measurements. While the outer sheath region and the inner core flow were anticipated prior to testing, the existence of a physically and optically thick layer composed of particulates and very high Na concentration was unexpected. In the FFC region the particulate component of the video signal presented a minor inconvenience for the LIF analysis by decreasing the effective dynamic range and producing a nonzero baseline in certain portions of the flow. However, the more important factor in the LIF analysis is the extreme optical depth of the FFC layer. In fact, it was found that at the Na line center frequency, the laser beam was totally absorbed. However, the laser beam did propagate through the FFC layer at frequencies off line center, and fluorescence was observed in both the particle layer and the inner core flow.

The video data acquired by Camera 1 from Test 3 at the 3-in.-downstream position, i.e., Laser 2, near the flow radial periphery displayed considerable Na fluorescence. As mentioned above, the data reduction process generates a spectral line at each point in the flow along the laser beam. The map given in Fig. 10 displays the Na fluorescence data of Camera 1, as was done in Fig. 5, with the frequency in the vertical dimension corresponding to −18 GHz and +12 GHz at the upper and lower edges, respectively, relative to the Na fluorescence line of the reference cell. The horizontal dimension is the field of view of Camera 1, corresponding to an absolute radial position in the flow from 58 to 98 cm relative to the nozzle centerline axis. The outermost plume fluorescence begins at ~ 94 cm. For radial positions between 90 and 88 cm in Fig. 10, the camera was saturated, and information on the peak intensity was lost. However, this represented

no significant loss of information, since the spectral fitting utilized the line wings. The centroid of the fluorescence displays a monotonic trend to more positive frequencies from 94 cm all the way to ~ 85 cm, at which point the velocity reaches a maximum. At positions interior 85 cm of Fig. 10, a given fluorescence line, i.e., a vertical or frequency profile, appears to have two peaks. This is simply due to the strong laser beam attenuation of the frequency-shifted line center by the optically dense outer portion of the flow. Yet there is considerable fluorescence in the wing of the Na line, indicating a high Na density. Inward of 78 cm, there is a precipitous drop in the Na density, indicating the boundary between the inner core flow and the particulate region discussed above. There is weak fluorescence in this region, although the S/N ratio is very small.

Vertical profiles of Fig. 10 were taken, analogous to those shown in Figs. 5 and 6, and it was found that in the very narrow region outside the FFC layer, the Na fluorescence displayed the usual hyperfine structure. However, as one moves further into the FFC layer, the optical depth significantly attenuates the line profile, precluding a simple determination of the gas static temperature in the FFC region. Spectra acquired within 78 cm, in the low Na density core flow, suffered from a low signal-to-noise ratio. This is largely due to the fact that only the far wings of the lines were obtainable since the kernel of the line was absorbed in the FFC region.

Even though the temperature was indeterminable in this flow, the radial velocity is rather insensitive to homogeneous line profile distortions. Hence, the spectral lines, using either the complete profile or only the wings as appropriate, were fit and a comparison was made to the predicted results, shown in Fig. 11 for Test 3. The agreement of the data with the prediction of the location and value of the radial velocity of the plume shear layer at the 3-in. axial position is quite satisfactory. It is interesting to note though, that the data indicate a slightly wider shear layer than the predictions. The sys-
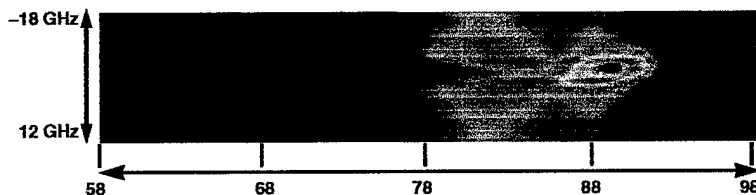

Fig. 10. Fluorescence signal acquired during one laser scan from LR91 Test 3.

tematic uncertainty of the radial velocity was estimated to be ± 10^4 cm/sec for a laser frequency scan period of slightly less than 5 seconds.
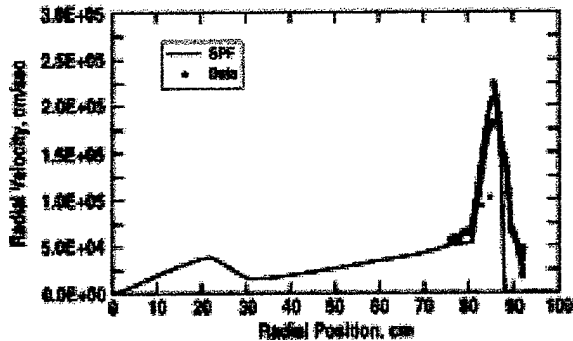

Fig. 11. Comparison of the measured radial velocity with the SPF predictions, Test 3.

The LIF data from Test 4 were manipulated in a similar manner as that of Test 3. However, in this case, Laser 1 (at the 6-in. axial position) was utilized. The character of Test 4 data is similar to that of Test 3, and only the final results are given here for brevity. A plot of the fit results for the radial velocity is given in Fig. 12. The results compare favorably with the predictions at 6 inches downstream of the nozzle exit. Curiously, the data seem to indicate a thinner shear layer than that predicted. As before, the optical depth of the FFC region was excessive in Test 4, and no accurate temperature information can be derived from these data.
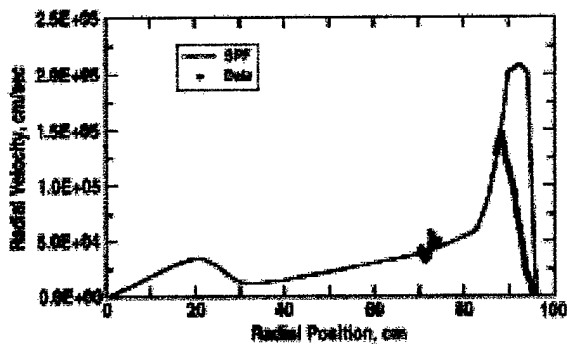

Fig. 12. Comparison of the measured radial velocity with the SPF predictions, Test 4.

In an attempt to identify the particles, the scattered laser beam profiles were averaged over 0.5-sec time intervals at times when the laser frequency was −18 GHz relative to the Na fluorescence center frequency. This resulted in the relative particle scattering profile as a function of radial

position. Because the camera gain settings were chosen to emphasize the fluorescence line wing structure while accepting the consequence of camera saturation at the spectral line center, it is possible that a small amount of Na fluorescence from the far wing of the fluorescence line is included in the particulate scattering profiles. However, since the Na fluorescence linewidth is of the order of only 1 to 2 GHz, the level of contribution of Na fluorescence to the signal measured at −18 GHz was assumed to be a minor effect, and was neglected.

The results for Test 3 at several times during the burn are shown in Fig. 13. All of these profiles were recorded at Station 1 (across the plume centerline) using Camera 1 (the boundary camera) and viewing Laser 2 (3 in. below the nozzle exit plane). From this plot, it appears that the scattering intensity distribution does not change over the first 30 sec of the burn, and the scattering intensity only slightly increases from the early to the late times of the burn. While the rise in intensity between early and late portions might be ascribed to an increase in ablative products, the very early detection and constant value of the profiles within the first 30 sec would argue against the origin of particles from the nozzle material.
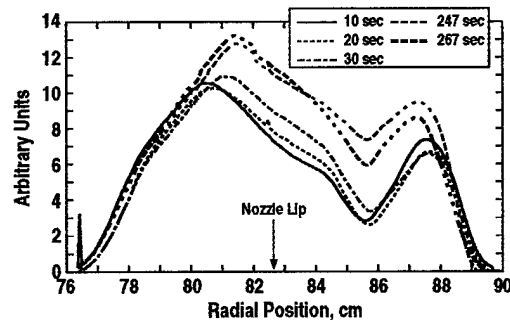

Fig. 13. Particle scattering in FFC region of LR91 plume, Test 3.

The particles were also observed in Tests 2 and 4, and the scattering intensity profiles are displayed in Fig. 14, along with the scattering intensity profile of Test 3. The profiles shown in Fig. 14 were obtained at 10 sec and the arbitrary units scale is the same for all tests. Since there were no significant temporal increases in profile intensity in Test 3 as a function of time, the comparison of the three tests at 10 sec should be valid. It is observed that

the double-peaked profile structure of Test 3 is replicated in Test 2, but not in Test 4. Furthermore, the spatial integrals of the particle scattering intensity profiles can be ranked as Test 3 having the highest integrated value, followed by Test 2, and then Test 4. This relation of the Test 3 value and the Test 2 value with the Test 4 value follows the trend of the amount of FFC present in the firings, as indicated in Table 2.

An analysis of the particulate scattering profiles at the 3-in. axial position during Test 4 was performed to assess the possible effects of the 7 chamber baffles on the uniformity of the flow. Figure 15a is a polar plot of the nozzle exit plane, as if viewing from above the engine, with the radial dimension corresponding to the distance from the nozzle axis. The curves show the radial location, in centimeters, of the maximum of the scattering
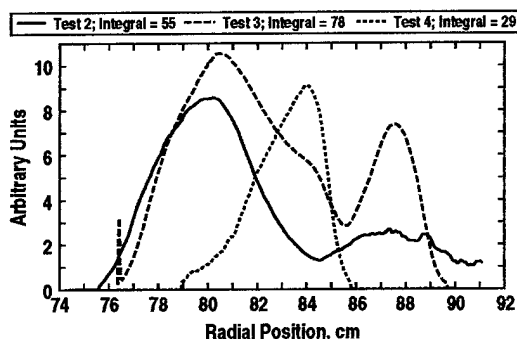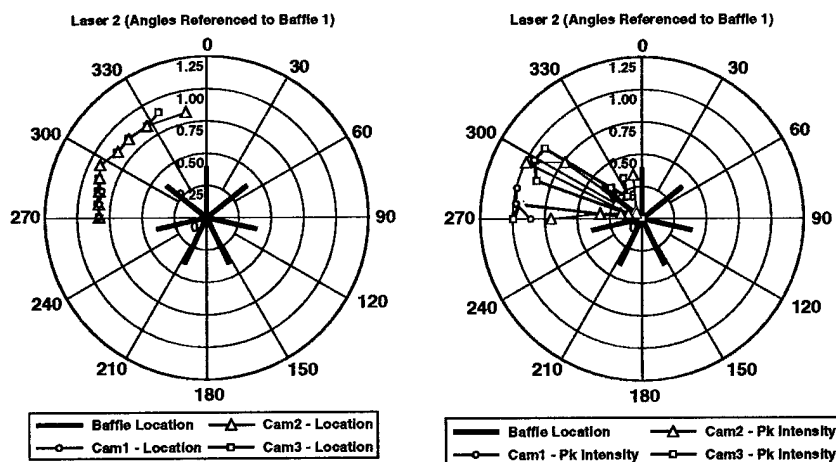

Fig. 14. Comparison of laser scattering profiles for Tests 2, 3, and 4.

intensity profile for each of the three cameras for the 10 traverse positions. The peak in the scattering is roughly 85 cm from the nozzle axis for all three cameras. Also shown are the approximate angular positions of the baffles, where the zero angular position is pointing directly to the position of the co-located full-field-of-view cameras (Cameras 2 and 3). As noted above, the boundary camera (Camera 1) acquired data on only the first 3 stations. The agreement of the radial location of the maximum of the scattering between the three independent cameras is excellent.

In addition to the spatial location of the peak of the scattering intensity profile, the angular variation of the peak value of the scattering intensity profile is of interest to assess the impact of the baffle structure upon the particle layer. For example, from Fig. 14, the spatial location of the peak of the Test 4 scattering intensity profile is at a radial position of roughly 84 cm, with an angular position of 270 deg, since it occurs at Station 1. Furthermore, the peak value of the scattering intensity profile, i.e., the value of the profile at 84 cm radial position and 270 deg, is roughly 9 arbitrary units. This information was tabulated for each of the 10 traverse stations, yielding the peak value of the scattering intensity profile as a function of the angular position of the observation. Figure 15b displays this function as a polar plot in which the radius is not the spatial dimension as in Fig. 15a, but the peak values of the scattering intensity profiles. Note that in order to facilitate comparisons between cameras, each curve was normalized, thus eliminating the effect of the differences in specific camera gain settings, etc. The angular variable in this plot still corresponds to the angular position around the nozzle as viewed from above the engine, as in Fig. 15a. The variation of the peak value of the scattering intensity profile as a function of angular position around the nozzle is quite dramatic in the full-field-of-view cameras (Cameras 2 and 3). Both sets of data

a. Radial location of maximum

b. Relative value of maximum

Fig. 15. Angular variation of the maximum scattering intensity for all cameras during Test 4 and 3 in. below nozzle exit.

show a clear maximum in the peak value of the scattering intensity profile at an angular position of roughly 300 deg, which is roughly near the estimated angular position corresponding to the chamber baffle at 306 deg. Furthermore, there is a definite minimum in the peak value of the scattering intensity profile for angular positions between the baffles, such as that seen at 280 and 325 deg. As mentioned above, the combustion chamber baffles are cooled by using fuel cooling near the intersections of the baffles with the chamber walls. Hence, this apparent rise in scattering intensity with baffle position is consistent with a higher level of fuel cooling produced by the baffles.

In addition to the laser scattering measurements, an absolute laser beam attenuation measurement was made, originally intended to verify the optically thin nature of the LR91 plume. In addition to a significant beam attenuation for laser frequencies near the Na fluorescence line, the laser beam was attenuated when the laser was spectrally far from the Na line center. This is interpreted as beam attenuation due to particle scattering. The attenuation and scattering measurements show a strongly correlated behavior in Fig. 16. This plot shows the measured beam attenuation at a laser frequency of −18 GHz, as compared to the spatially integrated particle scattering intensity for select times in the first 35 sec of Test 3. The strong (negative) correlation of the two independent measurements is evident and indicates that two independent measurement techniques observed the same phenomena. Not shown on the plot are the values of the curves when the traverse mechanism returns to Station 1 at the end of Test 3. These values are very similar to those plotted, and indicate
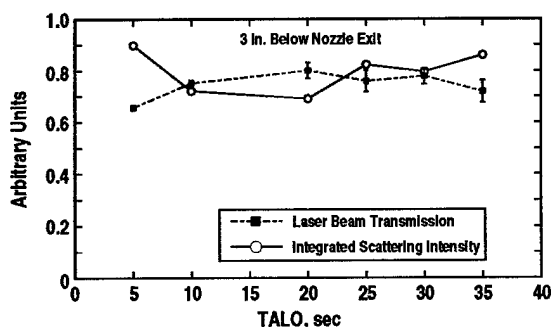
that the particle density is fairly constant in time throughout the burn.

The attenuation data was analyzed using Mie scattering theory to estimate a lower bound to the mass flow of particles exiting the nozzle. The most logical candidate for the particle identity was either AZ50 or quartz. The indices of refraction for AZ50 and quartz are very similar at 589 nm, and the present laser attenuation measurement would not be able to distinguish between the two on the basis of optical properties. However, by using the scattering data to define a path length, a bounding curve, Fig. 17, for the total mass flow was established as a function of particle diameter. Shown on this plot is the mass flow of AZ50 required to account for the measured laser transmission at 25 sec in Test 3, given that the particles are of a given monodisperse distribution size. (Note that quartz has a nearly identical bounding curve due to the similarity of the optical properties of quartz and AZ50.) Thus, a conservative estimate of the lower bound of the total mass flow would be to pick from the minimum of the curve, corresponding to approximately 200 gm/sec. This amount of AZ50 lost from the combustion cycle, which amounts to 0.4 percent of total fuel flow, is not sufficient to impact the system performance. Since, as noted above, the particle flux is roughly constant throughout the burn, the total mass expelled during Test 3 is estimated to be approximately 55 kg or 120 lb, assuming cylindrical symmetry of the particle distribution in the exhaust flow. Interestingly, the pre- and posttest weighings of the nozzle record a total weight loss of only 45.5 lb during the test. If stan-

Fig. 16. Variation in the laser scattering intensity, as compared to the measured beam attenuation for Test 3, Station 1.
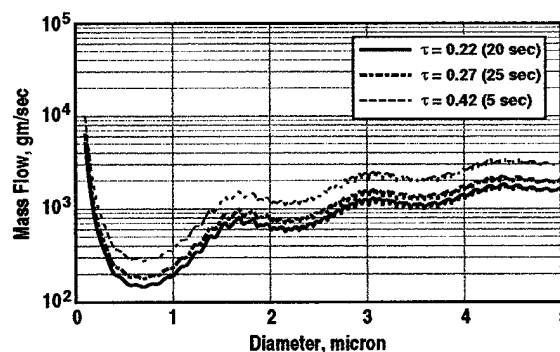

Fig. 17. Estimation of particle mass flow, based upon measured beam attenuation for Test 3, Station 1.

dard posttest bake-out analyses are followed which ascribe a nominal 13 percent of the weight loss to posttest evaporation, the maximum nozzle material loss during the firing due to nozzle charring is limited to 39.6 lb. Thus, based upon this crude estimate of the mass flow, it appears impossible that the sole source of the particles could be the nozzle liner material. Since the nozzle liner is designed to char without particle loss rather than ablate, this leaves AZ50 droplets in the FFC layer as the prime candidate for the observed scattering. Unfortunately, the attenuation measurement failed in Test 4.

Conclusions

Overall, the Na LIF measurements performed on two vastly different full-scale rocket engines in simulated altitude conditions were highly successful. The measurements were nonintrusive and yielded excellent radial velocity data, even in the difficult LR91 flow field. The accuracy of the flow temperature measurement requires further refinement, with proper accounting of the full temperature and pressure dependence of the saturation parameter. The residual effects of the combustion chamber and the nozzle, such as the baffle fuel cooling and nozzle wall heating, were observed to persist to the nozzle exit plane. From the OMS and LR91 data sets, it is evident that Na LIF probing of rocket flows has the potential to provide crucial information on nozzle design, thermal integrity, and combustor mixing and performance.

Specifically, the OMS engine operated in a very steady fashion, with the exit plane gas temperature maintaining a constant profile over the burn duration. The exception to this is the outer periphery, which clearly indicated the effects of the nozzle heating, or rather the loss of nozzle cooling ability as it began to heat, of the exhaust gas over time. The LR91 results were very constant over time in the flow periphery, due to the large FFC levels. The agreement of computational modeling of the shear layer with the data was encouraging, but identify areas for code improvement. Furthermore, the modeling of the centerline flow needs review for the case of the OMS engine. The data show a much more dynamic region, with the flow reversing radial direction twice near the core, and with signif-

icant magnitudes which were much greater than predicted. Also, some other minor features appeared in the data, due perhaps to weak shock waves that are not captured in the model. An important LR91 result is the observance of the AZ50 droplets in the flow. While this result was far from anticipated, the data are consistent with this identification. The estimation of the amount of AZ50 used the absolute laser attenuation taken at a position midway between the angular position of the combustion chamber baffles, where the scattering intensity was observed to increase dramatically compared to the midway position. Furthermore, the estimation assumed conservative lower bound estimates of particle sizes and optical properties. Thus, this estimate of the incomplete fuel vaporization may be drastically lower than the true amount, and more data are required to resolve this issue. Future assessments of particle behavior should use an optimized nonintrusive system. Should further measurements confirm the phenomena observed herein, then it may be possible to conceive of a dedicated test sequence which serves to define the minimum FFC level to operate the LR91, or other FFC engine, in order to maximize payload capabilities.

A desired improvement for future measurements is the reduction of the background signal in order to raise the LIF signal-to-noise ratio. In the LR91, the tradeoff to obtain the entire nozzle coverage at the expense of a narrow bandpass filter was too much in favor of the spatial coverage. In future efforts, a reduced field of view should be accepted, if need be, in favor of the narrow filters. For heavily fuel-film cooled rocket engines, the problem of optical depth remains, without a simple resolution. A possible alternative, which still exploits Na in the fuel, is to incorporate a pump-probe arrangement. Regardless, pretest efforts to quantify the amount of Na present in the fuel should be increased.

References

1. Aerojet-General Corporate Report No. LRP198, "Storable Liquid Propellants, Nitrogen Tetroxide/Aerozine 50," June 1962.

2. Schmidt, E. W., *Hydrazine and Its Derivatives*, John Wiley & Sons, NY,1984.

3. Yalin, A. P., et al., "Planar Imaging in a Mach 8 Flow using Sodium Laser-Induced Fluorescence," AIAA paper 96-2270, 19th AIAA Advanced Measurement and Ground Testing Conference, New Orleans LA, 1996.

4. Winker, B. K., and Wright, J. C., *Optics Letters*, **13**, 913 (1988).

5. Weiland, K. J. R., Wise, M. L., and Smith, G. P., *Applied Opics*, **32**, 4066 (1993).

6. "The Proceedings of the Workshop on Laser Diagnostics in Fluid Mechanics and Combustion," held at DSTO Aeronautical Research Laboratory, Fishermen Bend, Victoria, Australia, September 1993 AD-A272808.

7. Daily, J.W., and Chan, C., *Combustion and Flame*, **33** 47 (1978).; and references therein.

8. Fairbank, W. M., Hansch, T. W., and Schalow, A.L., *J. Opt. Soc. Am.,* **65** (1975).

9. Brasier, C. W. and Porter, R. G., "Development of a Laser-Induced Fluorescence System for Application to Rocket Plumes," AEDC-TR-92-6 (AD-A259760), January 1993.

10. Press, W. H., Flannery, B. P., Teukolsky, S.A., and Vetterling, W.T., *Numerical Recipes*, Cambridge University Press, 1986.

11. Cheng, S. S., "Resonant Doppler Velocimetry in Supersonic Nitrogen Flow," Ph.D. Dissertation, Princeton University,1982.

12. Demtroder, W., *Laser Spectroscopy,* Springer-Verlag, 1996 (Second Edition).

13. Nickerson, G. R., "Two-Dimensional Kinetics (TDK) Nozzle Performance Computer Program," NASA-36863, March 1989.

14. Wolf, D. E., Dash, S. M., and Pergament, H. S., "A Shock-Capturing Model for Two-Phase Chemically Reacting Flow in Rocket Nozzles," AIAA Paper No. 85-0306, Reno, NV, January 1985.

REPORT DOCUMENTATION PAGE

Form Approved
OMB No. 0704-0188

1. AGENCY USE ONLY *(Leave blank)*	2. REPORT DATE June 23-25, 1997	3. REPORT TYPE AND DATES COVERED Technical Society Paper

4. TITLE AND SUBTITLE
Laser-Induced Fluorescence Measurements of OMS and LR91 Amine Rocket Exhausts
AIAA Paper No. 97-2378

5. FUNDING NUMBERS
Job No. 0094

6. AUTHOR(S)
Brasier, C. W., Drakes, J. A., Anspach, K. M., Porter, R. G., Simmons, M. A., and Pruitt, D. W.

7. PERFORMING ORGANIZATION NAME(S) AND ADDRESS(ES)
Sverdrup Technology, Inc., AEDC Group
Arnold Engineering Development Center
Arnold AFB, TN 37389-9011

8. PERFORMING ORGANIZATION REPORT NUMBER

9. SPONSORING/MONITORING AGENCY NAME(S) AND ADDRESS(ES)
Arnold Engineering Development Center
Air Force Materiel Command
Arnold AFB, TN 37389-9011

10. SPONSORING/MONITORING AGENCY REPORT NUMBER

11. SUPPLEMENTARY NOTES
Presented at 28th Plasmadynamics and Lasers Meeting & Exhibit in Atlanta, GA.

12a. DISTRIBUTION AVAILABILITY STATEMENT
Approved for public release; distribution unlimited.

12b. DISTRIBUTION CODE

A

13. ABSTRACT *(Maximum 200 words)*
Nonintrusive diagnostics are often sought to provide information on combustion exhaust flows due to the harsh environment of the flow. Laser-induced fluorescence (LIF) is one technique in which a chosen flow molecule or marker is probed to yield gross flow properties such as static temperature and flow velocities. The work presented herein describes application of LIF to the combustion exhausts of two full-scale liquid-propellant rocket engines, i.e., the Space Shuttle Orbital Maneuvering System (OMS) and the Titan second-stage LR91 rocket engines, as they undergo routine testing in simulated altitude test cells. The method is based upon the use of cw ring-dye lasers which scan in frequency over either the Na D 1 or D 2 line at 5896 and 5890 Å. Na is used as a basis for this approach since it occurs as a trace element in both hydrogen and amine rocket fuels. The generic apparatus is described, including a discussion of the collection and interpretation of the LIF signal to yield radial and temporal profiles of radial flow velocity and static temperature. CFD modeling of the plumes was used to provide baseline estimates of the exhaust flow properties. It was found that the CFD model does a fairly good job of predicting the gross behavior of the flow, although some items of fine spatial structure are not reproduced well. The OMS and LR91 rocket engine nozzles are drastically different in construction and cooling method. It was found that excellent LIF results were obtained with the radiation-cooled nozzle (OMS), while the fuel-film cooling (FFC) used for the LR91 nozzle generated an optically thick and particle-laden region which severely impeded the determination of static temperature from the Na LIF measurements. Ancillary optical scattering measurements were made on the LR91 which indicated the existence

14. SUBJECT TERMS
laser-induced fluorescence, rocket plumes

15. NUMBER OF PAGES
16

16. PRICE CODE

17. SECURITY CLASSIFICATION OF REPORT	18. SECURITY CLASSIFICATION OF THIS PAGE	19. SECURITY CLASSIFICATION OF ABSTRACT	20. LIMITATION OF ABSTRACT
Unclassified	Unclassified	Unclassified	UL